Flexoelectricity in soft elastomers and the molecular mechanisms underpinning the design and emergence of giant flexoelectricity

Matthew Grasinger[a,b,1], Kosar Mozaffari[c,1], and Pradeep Sharma[c,d,2]

[a]Materials and Manufacturing Directorate, Air Force Research Laboratory, Wright-Patterson Air Force Base, OH 45433; [b]UES, Inc., Dayton, OH 45432; [c]Department of Mechanical Engineering, University of Houston, Houston, TX 77204; and [d]Department of Physics, University of Houston, Houston, TX 77204

Edited by Yonggang Huang, Northwestern University, Glencoe, IL, and approved March 29, 2021 (received for review February 8, 2021)

Soft robotics requires materials that are capable of large deformation and amenable to actuation with external stimuli such as electric fields. Energy harvesting, biomedical devices, flexible electronics, and sensors are some other applications enabled by electroactive soft materials. The phenomenon of flexoelectricity is an enticing alternative that refers to the development of electric polarization in dielectrics when subjected to strain gradients. In particular, flexoelectricity offers a direct linear coupling between a highly desirable deformation mode (flexure) and electric stimulus. Unfortunately, barring some exceptions, the flexoelectric effect is quite weak and rather substantial bending curvatures are required for an appreciable electromechanical response. Most experiments in the literature appear to confirm modest flexoelectricity in polymers although perplexingly, a singular work has measured a "giant" effect in elastomers under some specific conditions. Due to the lack of an understanding of the microscopic underpinnings of flexoelectricity in elastomers and a commensurate theory, it is not currently possible to either explain the contradictory experimental results on elastomers or pursue avenues for possible design of large flexoelectricity. In this work, we present a statistical-mechanics theory for the emergent flexoelectricity of elastomers consisting of polar monomers. The theory is shown to be valid in broad generality and leads to key insights regarding both giant flexoelectricity and material design. In particular, the theory shows that, in standard elastomer networks, combining stretching and bending is a mechanism for obtaining giant flexoelectricity, which also explains the aforementioned, surprising experimental discovery.

flexoelectricity | elastomers

Typical hard materials such as ceramics have elastic moduli on the order of several hundreds of gigapascals. Their deformation, under appropriate levels of mechanical forces, is barely discernible to the naked eye. On the other end of the spectrum, a change of area of nearly 1,700% has been demonstrated for an acrylic membrane (1). While both hard and soft materials have their respective usages, there are important technological imperatives to consider highly deformable soft materials. An oft-quoted example is that of a robotic appendage clasping and moving an object (Fig. 1). This requires the capability of large deformation. Ideally, we also hope that such a motion is accomplished through the application of a stimulus that is easily applied (e.g., an electrical field through a battery) and with a modest expenditure of energy. Soft materials that are highly deformable, tough (2), and respond easily to stimuli such as electric field (the focus of this work) have wide applications: biomedical prostheses and devices (3–7), shape-conforming sensors (8–11), energy harvesting (12–14), stretchable electronics (15–18), and, of course, robotics (12, 19, 20). As a compelling illustration of applications, we refer the reader to fascinating recent works on using magnetic actuation to achieve a soft robot made essentially of a rubber filament that is capable of being steered through the complex cerebrovascular system with aneurysms (20).

The electromechanical coupling that we hope for a soft material to possess is piezoelectricity. Materials that are piezoelectric permit a direct and a linear relation between the development of an electric field and subjected mechanical stress, and vice versa. Piezoelectricity can be shown by a linearized relation between polarization ($\mathbf{P}$) and the strain tensor ($\boldsymbol{\varepsilon}$) as $P_i \approx \mathcal{D}_{ijk}\varepsilon_{jk}$, where $\mathcal{D}$ is a third-order tensor reflecting the piezoelectric properties of the material. Unfortunately, piezoelectricity requires the atomic structure of the material to conform to a rather stringent set of symmetry conditions found only in certain hard ceramics. The rather few piezoelectric polymers such as polyvinylidene difluoride (PVDF) are (relatively speaking) fairly stiff.* Therefore, the electromechanical coupling mechanism that we rely on in the context of soft dielectric elastomer is the Maxwell stress effect or electrostriction—indeed, these are the precise mechanisms operative in the example we quoted in the preceding paragraph involving the nearly 1,700% areal increase in the acrylic membrane (1). Both the Maxwell stress effect and electrostriction are universally present in all dielectrics where the induced mechanical strain ε scales with the square of the applied electric field E^2. There is no converse effect; hence, applications such as energy harvesting and sensing are not eas-

Significance

The molecular-scale phenomena that lead to the emergence of the flexoelectric effect in elastomers are not well understood. We present a molecular-to-continuum scale theory and show it to be valid for common types of elastomers. We unravel a mechanism for achieving giant flexoelectricity—which finds support in prior experimental results. The multiscale theory is then leveraged for material design and we propose specific modalities for 1) the emergence of piezoelectricity, 2) tuning the direction of flexoelectricity, and 3) flexoelectricity which is invariant with respect to spurious deformations. These developments may pave the way for the future development of efficient soft energy harvesters, sensors, and actuators, and may prove useful for high-degree-of-freedom soft robots and artificial muscles.

Author contributions: P.S. designed research; M.G. and K.M. performed research; M.G., K.M., and P.S. analyzed data; and M.G., K.M., and P.S. wrote the paper.

The authors declare no competing interest.

This article is a PNAS Direct Submission.

[1]M.G. and K.M. contributed equally to this work.

[2]To whom correspondence may be addressed. Email: psharma@uh.edu.

This article contains supporting information online at https://www.pnas.org/lookup/suppl/doi:10.1073/pnas.2102477118/-/DCSupplemental.

Published May 21, 2021.

*Their elastic modulus is on the order of a few gigapascals, while the soft materials that are highly deformable often need to have stiffness in the kilopascal range.

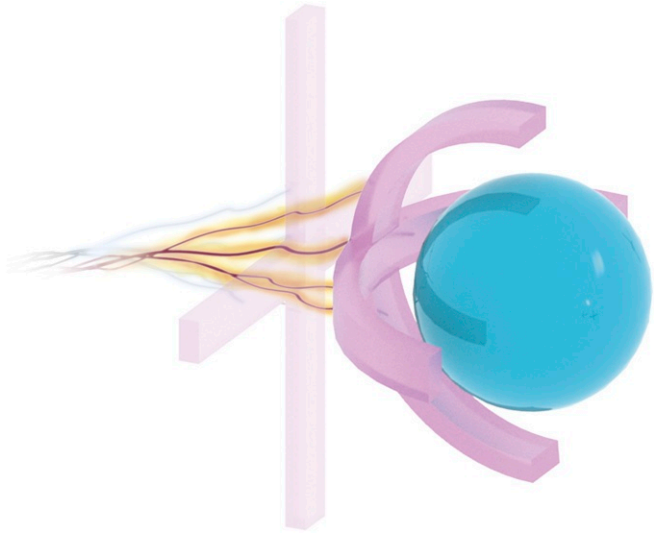

Fig. 1. Schematic of a soft robotic appendage, deforming in order to grab an object due to electrical stimuli.

ily possible. Further, rather high electric fields must be imposed to generate sufficient forces for an appreciable actuation. An exciting alternative is to embed frozen charges and dipoles in soft matter to create so-called electrets (21–26). Through the interaction of preexisting immobile charges, electrostriction, and the inherent softness of the material, electrets effectively act as piezoelectrics.[†] While this is a promising research avenue, a key impediment in the use and development of electret materials is that the frozen external charges are only metastable and have a propensity to leak out—especially at elevated temperatures and under humid conditions (30).

Having established the relevant context regarding electromechanical coupling mechanisms in soft materials, we now turn to a yet another phenomenon—flexoelectricity—which has generated much recent attention (31–33). Briefly, it is the coupling between polarization and strain gradients and can be illustrated by $P_i \approx f_{ijkl}\,(\partial \varepsilon_{jk}/\partial x_l)$, where $\boldsymbol{f}$ is a fourth-order tensor embodying the flexoelectric behavior of the material. Like electrostriction, flexoelectricity is also a universal phenomenon which occurs in all insulating materials. In nonpiezoelectrics, the symmetry of the charge density throughout the material is such that the dipole moment per unit volume, that is, polarization, vanishes. A homogeneous deformation cannot break the symmetry of the ground-state charge density; however, strain gradients can and do, thereby inducing polarization. Very interestingly, the flexoelectric effect has been used to create apparently piezoelectric materials without using piezoelectric materials (33–36) and has broad-ranging applications in energy harvesting (37–42), and sensors and actuators (43–46). The phenomenon also appears to be implicated in several biophysical functions, for example, the mammalian hearing mechanism (47–49). A notable aspect of flexoelectricity is the associated size effect (31). The developed polarization due to flexoelectricity scales with the gradient of the strain. Large strain gradients are most easily produced when feature size is small (e.g., beam thickness, size of embedded inclusions in a composite), and, indeed, at least for hard materials, the phenomenon becomes appreciable only at the nanoscale. For soft matter, due to the corresponding lower elastic modulus, a nontrivial flexoelectric response is even possible at micron-length scales (41, 50, 51). As a notable example, Deng et al. (50) exploited flexoelectricity to design soft materials whose apparent piezoelectric strength is nearly 20 times greater than the hard ferroelectrics like barium titanate with feature sizes on the order of 0.6 μm.

The phenomenological theory of flexoelectricity, with various degrees of sophistication and nuances, appears to be now well developed (e.g., refs. 32, 52, and 53). In the context of soft matter, a first attempt appeared in ref. 50, and we highlight a more recent paper, ref. 53, that is specifically targeted toward proper accounting for large deformations and the correct interpretation of the flexoelectric matter property tensor for large deformations. Significant efforts have also been expended toward computational approaches (e.g., refs. 53–56). At the other end of the scale spectrum, extensive research has also ensued on the microscopic underpinnings of the phenomenon. The atomistic-scale mechanisms for flexoelectricity are now relatively well understood for crystalline materials (57–61), liquid crystals (62, 63), and two-dimensional (2D) materials (64–69). However, a similar molecular-scale understanding of the flexoelectricity of elastomers has remained elusive (31). This is a key impediment in the design of next-generation soft materials that exhibit substantive flexoelectricity. The flexoelectric coefficients of most soft polymers (like elastomers) exhibit rather modest values. Attempts were made, in refs. 70 and 71, to explain flexoelectricity in elastomers through quasi-1D microscopically based models which utilized linear elastic chains connecting neutral, positive, and negative ions and a kind of free volume theory, respectively. These models are useful to assess the order of magnitude of the flexoelectric effect in elastomers but can hardly capture the nuances of the actual mechanisms and thus are of limited utility for designing materials. The state of affairs is complicated further by experiments which indicate a wide range of flexoelectricity in polymers (72, 73). In this work, we take inspiration from the fact that statistical mechanics and polymer network modeling have explained much of what we understand about the microscopic underpinnings of elasticity (74–77) in elastomers. More recently, a similar success has also been achieved in the context of electroelasticity (78–80), which has inspired our current approach.

In this work, we do the following.

1) We create a molecular-scale theory for the emergent flexoelectricity of elastomers with polar monomers. The molecular-scale theory is quite general; it is valid for two of the most common theoretical models for polymers: the freely jointed chain and the wormlike chain.
2) We provide an explanation for the rather wide and nonintuitive range of flexoelectric properties measured for polymers and specifically explain the unusually large values obtained when stretching and bending are combined.
3) We provide an interpretation of understanding microscopic flexoelectricity using the notion of quadrupolar moments and leverage this connection to develop material design principles for tuning the direction of the flexoelectric effect, as well as for stretch-invariant flexoelectricity.
4) Finally, we provide simple and clear guidelines to design soft elastomers with giant flexoelectricity.

Statistical Mechanics of the Electroelasticity of a Freely Jointed Chain

As a starting point, we derive the free energy of a polymer chain in a fixed ambient temperature, T, with a fixed end-to-end vector, $\boldsymbol{r}$, subjected to a constant electric field, $\boldsymbol{E}$. We work in the constant electric field ensemble as a matter of convenience and will eventually use a Legendre transformation to arrive at the Helmholtz free energy. To work in this ensemble, we need the

[†]Detailed theoretical framework outlining the conditions for when electrets act a piezoelectric or even pyroelectric are available in refs. 26 and 27. Other illustrative examples may be found in the literature (25, 28, 29).

variation of the electric field due to the presence of monomer dipoles to be negligible; that is, the monomers need to be approximately noninteracting.[‡] Such an assumption is quite reasonable; compare ref. 81 and *SI Appendix*, section 1, where we use Markov chain Monte Carlo calculations to prove this point.

We assume that the energy required to deform an individual monomer is much greater than kT, and, hence, we model the monomers as rigid with length b. For the freely jointed chain, monomers are also free to rotate about their neighboring bonds. We denote the number of monomers per chain as n, the chain stretch as $\gamma := r/nb$, and the orientation of a monomer as $\hat{\boldsymbol{n}}$ so that $\boldsymbol{r} = b\sum_{i=1}^{n}\hat{\boldsymbol{n}}_i$. By assumption, the monomers are polar, or, in other words, have a permanent dipole attached to them. In general, the dipole vector, $\boldsymbol{\mu}$, need not be aligned with $\hat{\boldsymbol{n}}$. However, we do assume that the dipole is a linear transformation of $\hat{\boldsymbol{n}}$; that is, $\boldsymbol{\mu} = \boldsymbol{M}\hat{\boldsymbol{n}}$. If, for example, a dipole of fixed magnitude is attached rigidly to the monomer such that it rotates with the monomer, then $\boldsymbol{M} = \mu\boldsymbol{Q}$, where $\boldsymbol{Q} \in \mathrm{SO}(3)$. In any case, the electric potential of a monomer depends on its orientation. Let $\boldsymbol{\mathcal{E}} := \boldsymbol{M}^T\boldsymbol{E}$. Then the electric potential of a monomer is given by the expression

$$u = -\boldsymbol{\mu}\cdot\boldsymbol{E} = -(\boldsymbol{M}\hat{\boldsymbol{n}})\cdot\boldsymbol{E} = -\boldsymbol{\mathcal{E}}\cdot\hat{\boldsymbol{n}}. \qquad [1]$$

In order to formulate the partition function, we divide the unit sphere into $\mathcal{N}$ infinitesimal patches of area with unit normal $\hat{\boldsymbol{n}}_i, i = 1, 2, \ldots, \mathcal{N}$. Let m_i denote the number of monomers in the chain with direction $\hat{\boldsymbol{n}}_i$. Then,

$$\mathcal{Z} = \sum_{\{m_j\}'}\left\{\exp\left[\beta\sum_{i=1}^{\mathcal{N}} m_i\boldsymbol{\mathcal{E}}\cdot\hat{\boldsymbol{n}}_i\right]\frac{n!}{\prod_{i=1}^{\mathcal{N}} m_i!}\right\}, \qquad [2]$$

where $\beta = 1/kT$, and the prime over $\{m_j\}$ denotes that the summation is over all of the collections of population numbers that satisfy the constraints: $\sum_i m_i = n$ and $b\sum_i m_i\hat{\boldsymbol{n}}_i = \boldsymbol{r}$. Enumerating over all of the terms in Eq. **2** is difficult, in general. Instead, we approximate the logarithm of the sum by the logarithm of its maximum term and, taking $\mathcal{N}\to\infty$ (i.e., the continuum limit of the population numbers), arrive at a mean-field theory. In doing so, we find that

$$\rho(\hat{\boldsymbol{n}}) = C\exp[\beta\boldsymbol{\mathcal{E}}\cdot\hat{\boldsymbol{n}} + \boldsymbol{\tau}\cdot\hat{\boldsymbol{n}}], \qquad [3]$$

where ρ is a probability density function associated with finding a monomer with some direction $\hat{\boldsymbol{n}}$, and C and τ are Lagrange multipliers that are determined by enforcing the continuum analog of the normalization and end-to-end vector constraints, respectively,

$$n = \int_{\mathbb{S}^2}\mathrm{d}A\,\rho, \quad \frac{\boldsymbol{r}}{b} = \int_{\mathbb{S}^2}\mathrm{d}A\,\rho\hat{\boldsymbol{n}}. \qquad [4]$$

Once the unknown multipliers have been determined, the closed-dielectric free energy, $\mathcal{F}$, is approximately

$$\mathcal{F} = -\frac{1}{\beta}\ln\mathcal{Z} \approx \int_{\mathbb{S}^2}\mathrm{d}A\,\rho u + \frac{1}{\beta}\int_{\mathbb{S}^2}\mathrm{d}A\,\rho\ln\rho. \qquad [5]$$

Let $\boldsymbol{\xi} := \beta\boldsymbol{\mathcal{E}} + \boldsymbol{\tau}$. Then the solution for C and $\boldsymbol{\xi}$ is well known (82), and

$$C = \frac{n\xi\,\mathrm{csch}\,\xi}{4\pi}, \quad \boldsymbol{\xi} = \mathcal{L}^{-1}(\gamma)\hat{\boldsymbol{r}}, \qquad [6]$$

where $\xi = |\boldsymbol{\xi}|$, $\hat{\boldsymbol{r}} = \boldsymbol{r}/r$, and $\mathcal{L}^{-1}$ is the inverse Langevin function. Based on cursory examination of Eq. **6**, it may seem somewhat surprising that ρ is independent of the electric field and is, in fact, equivalent to the ρ that maximizes the entropy. However, it is easy to show that this is indeed the ρ which minimizes the free energy for any monomer potential energy which is linear in $\hat{\boldsymbol{n}}$. To show this, let ρ' be any function which satisfies the constraints, Eq. **4**, and let $u(\hat{\boldsymbol{n}}) = \alpha + \mathbf{A}\hat{\boldsymbol{n}}$. Now, we can perturb ρ with some arbitrary function $\delta\rho(\hat{\boldsymbol{n}})$ and still satisfy the constraints provided,

$$\int_{\mathbb{S}^2}\mathrm{d}A\,\delta\rho = 0, \quad \int_{\mathbb{S}^2}\mathrm{d}A\,(\delta\rho)\hat{\boldsymbol{n}} = 0. \qquad [7]$$

Then the change in internal energy due to $\rho\to\rho+\delta\rho$ is

$$\int_{\mathbb{S}^2}\mathrm{d}A\,(\rho+\delta\rho)u - \int_{\mathbb{S}^2}\mathrm{d}A\,\rho u = \int_{\mathbb{S}^2}\mathrm{d}A\,(\delta\rho)(\alpha + \mathbf{A}\hat{\boldsymbol{n}}),$$

which vanishes by Eq. **7**. Therefore, if the monomer potential energy is linear in $\hat{\boldsymbol{n}}$, then all ρ which satisfy Eq. **4** have the same internal energy. In conclusion, we infer that, in this case, the density which minimizes the free energy is the same as that which maximizes the entropy.

Next, using Eqs. **6** and **3** in Eq. **5**, we obtain the chain free energy,

$$\mathcal{F} = n\left[\frac{1}{\beta}\left(\gamma\xi + \ln\frac{\xi\,\mathrm{csch}\,\xi}{4\pi}\right) - \gamma(\boldsymbol{\mathcal{E}}\cdot\hat{\boldsymbol{r}})\right]. \qquad [8]$$

Finally, we define the chain polarization as $\boldsymbol{p} = \int_{\mathbb{S}^2}\mathrm{d}A\,\rho\boldsymbol{\mu}$. It is easy to show that $-\partial\mathcal{F}/\partial\boldsymbol{E} = \boldsymbol{p}$.[§] Thus,

$$\boldsymbol{p} = \boldsymbol{M}\frac{\boldsymbol{r}}{b} = n\gamma\boldsymbol{M}\hat{\boldsymbol{r}}, \qquad [9]$$

where $\hat{\boldsymbol{r}} = \boldsymbol{r}/r$. By Eq. **9**, the chain polarization is determined uniquely by the chain end-to-end vector, irrespective of the temperature or the electric field. In addition, since $\gamma\in[0,1]$, we have that $p\in[0, n\kappa(\boldsymbol{M})]$, where $\kappa(\square)$ is the spectral radius of $\square$. If $\boldsymbol{M} = \mu\boldsymbol{Q}$, then the maximum polarization simplifies to $n\mu$ and occurs when the chain is fully stretched. Importantly, despite the fact that dipole–dipole interactions were assumed negligible in deriving Eq. **9**, we note that Markov chain Monte Carlo simulations agree with Eq. **9** nearly exactly, even when dipole–dipole interactions are significant (*SI Appendix*, section 1).

Statistical Mechanics of the Electroelasticity of a Wormlike Chain

Ultimately, because we are interested in what universal phenomena may arise from all polymer chains with polar monomers—not just those that behave as freely jointed chains—we next consider polar monomers in a wormlike chain. By wormlike chain, we mean a chain which again consists of rigid monomers but has some bending stiffness along its contour. That is, the bond which joins monomer i to monomer $i+1$ has rotational stiffness K_i. Recalling $\boldsymbol{\mathcal{E}} := \boldsymbol{M}^T\boldsymbol{E}$, the Hamiltonian reads

$$\mathcal{H} = \sum_{i=1}^{n}\left(\frac{K_i}{2b}(\hat{\boldsymbol{n}}_{i+1} - \hat{\boldsymbol{n}}_i)^2 - \boldsymbol{\mathcal{E}}\cdot\hat{\boldsymbol{n}}_i\right), \qquad [10]$$

where it is assumed that $K_n = 0$ to simulate a hinged boundary condition (at the chain's end). In the limit of $b\to 0$ and $n\to\infty$,

[‡] To be precise, we assume that the energy of dipole–dipole interactions is small relative to the thermal energy of the chain, nkT. An order of magnitude estimate for this condition can be obtained from dimensional analysis: $\tilde{\mu}^2 \ll 1$, where $\tilde{\mu} := \mu/\sqrt{\epsilon_0 b^3 kT}$, and μ is a characteristic dipole magnitude.

[§] In general, the relationship between $\boldsymbol{E}$ and $\boldsymbol{p}$ requires solving a nonlocal boundary value problem. However, when dipole–dipole interactions are negligible, the nonlocal relationship simplifies to the local one given in ref. 81.

Eq. **10** becomes

$$\mathcal{H} \simeq \int_0^L \left(\frac{K(s)}{2} \left| \frac{\mathrm{d}\hat{\boldsymbol{n}}}{\mathrm{d}s} \right|^2 - \frac{1}{b} \boldsymbol{\mathcal{E}} \cdot \hat{\boldsymbol{n}} \right) \mathrm{d}s, \qquad [11]$$

where $L = nb$ is the chain length, and the chain is parameterized by its arclength, $s \in [0, L]$. For simplicity, we assume that the stiffness is same throughout the chain, that is, $K(s) = K$.

Here we again consider a fixed end-to-end vector ensemble. Formally, the end-to-end vector and normalization constraints are

$$\begin{aligned} \boldsymbol{g}[\hat{\boldsymbol{n}}] &= \frac{1}{L} \left(b \sum_{i=1}^{n} \hat{\boldsymbol{n}}_i - \boldsymbol{r} \right) \simeq \frac{1}{L} \int_s \hat{\boldsymbol{n}} \, \mathrm{d}s - \frac{\boldsymbol{r}}{L} = \boldsymbol{0}, \\ h(s) &= \hat{\boldsymbol{n}}_i \cdot \hat{\boldsymbol{n}}_i - 1 \simeq \hat{\boldsymbol{n}}(s) \cdot \hat{\boldsymbol{n}}(s) - 1 = 0. \end{aligned} \qquad [12]$$

Let $\boldsymbol{g}[\hat{\boldsymbol{n}}] = (g_1, g_2, g_3)$; when evaluating the partition function, the constraints are enforced through Dirac delta distributions (83) and functionals (84),

$$\mathcal{Z} = \int \exp[-\beta \mathcal{H}] \, \delta(g_1) \delta(g_2) \delta(g_3) \delta[h] \, \mathcal{D}\hat{\boldsymbol{n}}.$$

Using the Fourier space representations of the Dirac delta distributions and functional (84), we have

$$\mathcal{Z} = \frac{1}{(2\pi)^4} \int \exp\left[-\beta \mathcal{H}^{\mathrm{eff}} \right] \mathrm{d}^3\boldsymbol{k} \, \mathcal{D}\gamma \, \mathcal{D}\hat{\boldsymbol{n}}, \qquad [13]$$

where $\boldsymbol{k} = \{k_1, k_2, k_3\}$ and $\gamma = \gamma(s)$ are wave vectors, and where the effective Hamiltonian is defined as

$$\begin{aligned} \mathcal{H}^{\mathrm{eff}} \simeq \int_0^L \left(\frac{K}{2} \left| \frac{\mathrm{d}\hat{\boldsymbol{n}}}{\mathrm{d}s} \right|^2 - \frac{1}{b} \boldsymbol{\mathcal{E}} \cdot \hat{\boldsymbol{n}} - \frac{i}{L\beta} \boldsymbol{k} \cdot \hat{\boldsymbol{n}} \right) \mathrm{d}s \\ + \frac{i}{L\beta} \boldsymbol{k} \cdot \boldsymbol{r} - \int_0^L \frac{i}{L\beta} \gamma(s) \left(\hat{\boldsymbol{n}} \cdot \hat{\boldsymbol{n}} - 1 \right) \mathrm{d}s. \end{aligned} \qquad [14]$$

The last term in Eq. **14** is anharmonic, and therefore makes Eq. **13** difficult, if not impossible, to evaluate exactly. As a result, we proceed to approximate the partition function by dropping the normalization constraint; that is, we let $\gamma(s) \to 0$. This elimination is equivalent to allowing the monomers to stretch or contract. We show, in *SI Appendix*, section 2, by using a variational approach, that this assumption (interestingly) does not alter our result.

Next, to evaluate (the harmonic approximation of) $\mathcal{Z}$, we use the Fourier transform of $\hat{\boldsymbol{n}}(s)$ given by

$$\hat{\boldsymbol{n}}(s) = \sum_{q \in \mathbb{K}} \boldsymbol{\omega}(q) \exp[iqs], \qquad [15]$$

where $\mathbb{K} = \{q : q = 2n\pi/L, n \in \mathbb{Z}, q_{min} \le |q| \le q_{max}\}$, $q_{min} = 0$, and $q_{max} = 2\pi/b$. The amplitudes of each mode $\boldsymbol{\omega}(q)$ can be achieved by

$$\boldsymbol{\omega}(q) = \frac{1}{L} \int_0^L \hat{\boldsymbol{n}}(s) \exp[-iqs] \mathrm{d}s. \qquad [16]$$

By definitions Eqs. **15** and **16**, we rewrite the effective Hamiltonian in Eq. **14** as follows:

$$\begin{aligned} \mathcal{H}_0^{\mathrm{eff}} = L \sum_{q \in \mathbb{K}} \left(\frac{K}{2} q^2 |\boldsymbol{\omega}(q)|^2 \right) - \frac{L}{b} \boldsymbol{\mathcal{E}} \cdot \boldsymbol{\omega}(0) \\ - \frac{i}{\beta} \boldsymbol{k} \cdot \boldsymbol{\omega}(0) + \frac{i}{L\beta} \boldsymbol{k} \cdot \boldsymbol{r}, \end{aligned} \qquad [17]$$

where $\mathcal{H}_0^{\mathrm{eff}}$ is the effective Hamiltonian upon dropping the normalization constraint, and $\boldsymbol{\omega}(0) = \boldsymbol{r}/L$ by definition. Notice that the partition function is now harmonic in the unknowns. Indeed, introducing $\boldsymbol{\alpha}(q, k) = [\omega_1(q_{min} : q_{max}), \omega_2(q_{min} : q_{max}), \omega_3(q_{min} : q_{max}), k_1, k_2, k_3]$, where Size $(\boldsymbol{\alpha}) =: m$, we rewrite Eq. **17** as a quadratic function with the linear term

$$\beta \mathcal{H}_0^{\mathrm{eff}} = \sum_{i,j=1}^{m} \frac{1}{2} \alpha_i A_{ij} \alpha_j + b_i \alpha_i, \qquad [18]$$

where $\boldsymbol{A}$ and $\boldsymbol{b}$ can be achieved from Eq. **17** by straightforward calculation. Plugging Eq. **18** into Eq. **13**,

$$\begin{aligned} \mathcal{Z}_0 &= \frac{1}{(2\pi)^4} \int \exp\left[-\beta \mathcal{H}_0^{\mathrm{eff}} \right] \mathrm{d}^m \boldsymbol{\alpha}, \\ &= \frac{1}{(2\pi)^4} \sqrt{\frac{(2\pi)^m}{\prod_{|q| \in \mathbb{K} \& q \neq 0} (2L\beta K |q|^2)^3}} \exp\left[\frac{\beta}{b} \boldsymbol{\mathcal{E}} \cdot \boldsymbol{r} \right]. \end{aligned} \qquad [19]$$

Once the partition function is obtained, we can identify the free energy of the system as follows:

$$\mathcal{F} = -\frac{1}{\beta} \ln(\mathcal{Z}_0) = \mathrm{const} + \frac{3}{2\beta} \sum_{|q| \in \mathbb{K} \& q \neq 0} \ln(2L\beta K |q|^2) - \frac{1}{b} \boldsymbol{\mathcal{E}} \cdot \boldsymbol{r}.$$

Thus recalling $\boldsymbol{\mathcal{E}} := \boldsymbol{M}^T \boldsymbol{E}$, by definition, the polarization can be achieved by

$$\boldsymbol{p} = -\frac{\partial \mathcal{F}}{\partial \boldsymbol{E}} = \boldsymbol{M} \frac{\boldsymbol{r}}{b} = n\gamma \boldsymbol{M} \hat{\boldsymbol{r}}, \qquad [20]$$

which is identical to Eq. **9**. We remark, as already noted earlier, that accounting for normalization constraint does not change the polarization of the system.

In the remainder of the work, we show that the stretch–polarization relationship (i.e., the relationship between a chain's end-to-end vector and its net dipole) is a key component of the flexoelectric effect of elastomers consisting of polar monomers. By Eqs. **9** and **20**, we can see that this relationship is consistent for both freely jointed and wormlike chains, and is invariant with respect to the ambient temperature or applied electric field. Further, although the analytical expressions were determined by assuming negligible dipole–dipole interactions, Monte Carlo simulations agree nearly exactly, even when dipole–dipole interactions are significant (*SI Appendix*). This surprisingly consistent result is a consequence of the monomer dipole constitutive response and the correspondence between thermodynamic state variables and ensemble averages. Indeed, let $\langle \square \rangle$ denote the ensemble average of $\square$. Then, the same relationship can be obtained almost by definition,

$$\begin{aligned} \boldsymbol{r} &= b \left\langle \sum_{i=1}^{n} \hat{\boldsymbol{n}}_i \right\rangle, \\ \boldsymbol{p} &= \left\langle \sum_{i=1}^{n} \boldsymbol{\mu}_i \right\rangle = \boldsymbol{M} \left\langle \sum_{i=1}^{n} \hat{\boldsymbol{n}}_i \right\rangle = \boldsymbol{M} \frac{\boldsymbol{r}}{b}. \end{aligned}$$

The broad applicability of the monomer dipole constitutive model [i.e., dipolar molecules are not uncommon (85)] and the consistency of the stretch–polarization relationship together suggest that the theory developed herein is potentially quite general; that is, it is expected to be valid for a wide range of types of elastomers, and for a variety of loading and environmental conditions.

Network Polarization: Coarse Graining from Chain Scale to the Continuum Scale

In coarse graining from the chain scale to the continuum scale, we assume that each material point can be represented by a prob-

ability distribution of chains and that these chains are in weak interaction with each other [that is, the free energy density at a material point is approximately the product of the average chain free energy—as if the chains were in isolation—and the density of chains per unit volume (86)]. This assumption is standard in elastomer elasticity (74, 77, 87–89), and has been used recently in elastomer electroelastictiy (78–80, 90). It is also consistent with our assumption that monomer–monomer interactions are negligible within a chain itself. Let $\langle\square\rangle_{\boldsymbol{r}}$ denote the average of $\square$ over chains in the current configuration. Then, by the weak interaction assumption, the closed-dielectric free energy density, $\mathcal{W}^*$, at a material point is

$$\mathcal{W}^* = N\,\langle\mathcal{F}\rangle_{\boldsymbol{r}}\,, \qquad [21]$$

where N is the number of chains per unit volume. Similarly, we take the (continuum-scale) polarization (i.e., dipole moment per unit volume), $\boldsymbol{P}$, as the average over chain polarizations; that is,

$$\boldsymbol{P} = N\,\langle\boldsymbol{p}\rangle_{\boldsymbol{r}} = N\boldsymbol{M}\left\langle\frac{\boldsymbol{r}}{b}\right\rangle_{\boldsymbol{r}}. \qquad [22]$$

Note that, as a consequence of Eqs. **5** and **22**, and, since averaging is a linear operation, $\boldsymbol{P} = -\partial\mathcal{W}^*/\partial\boldsymbol{E}$.[¶] This result, in congruence with a rigorous thermodynamic treatment of the consequences of deriving the chain-scale free energy in a fixed electric field ensemble, leads us to the conclusion that $\mathcal{W}^*$ is the Legendre transform (with respect to polarization) of the Helmholtz free energy density, $\mathcal{W}$. Thus,

$$\mathcal{W} = \mathcal{W}^* - \boldsymbol{P}\cdot\boldsymbol{E}. \qquad [23]$$

The chain averaging considered thus far has been in the current configuration. To, instead, understand these quantities in terms of the reference configuration and continuum-scale deformations, we must make a kinematic assumption regarding how chains in the reference configuration are mapped into the current configuration.[#] Here we assume that chain end-to-end vectors are mapped from the reference to the current configuration under the deformation gradient, $\boldsymbol{F}$. In the literature, this is known as the affine deformation assumption (74).

Finally, let $\langle\square\rangle_{\tilde{\boldsymbol{r}}}$ denote the average of $\square$ over chains in the reference configuration, $J := \det\boldsymbol{F}$, $N_0 := JN$, and $\tilde{\boldsymbol{P}} := J\boldsymbol{P}$. (We say that $\tilde{\boldsymbol{P}}$ is the pullback of $\boldsymbol{P}$.) Then

$$\begin{aligned}\mathcal{W}^*(\boldsymbol{F};\boldsymbol{E}) &= N_0\,\langle\mathcal{F}(\boldsymbol{F}\tilde{\boldsymbol{r}},\boldsymbol{E})\rangle_{\tilde{\boldsymbol{r}}}\,,\\ \mathcal{W}(\boldsymbol{F};\boldsymbol{E}) &= \mathcal{W}^*(\boldsymbol{F},\boldsymbol{E}) - J^{-1}\tilde{\boldsymbol{P}}(\boldsymbol{F})\cdot\boldsymbol{E},\\ \tilde{\boldsymbol{P}}(\boldsymbol{F}) &= N_0\,\langle\boldsymbol{p}(\boldsymbol{F}\tilde{\boldsymbol{r}})\rangle_{\tilde{\boldsymbol{r}}}\,,\end{aligned}$$

where we write $\tilde{\boldsymbol{P}} = \tilde{\boldsymbol{P}}(\boldsymbol{F})$ to reinforce the fact that, in the case when monomer–monomer and chain–chain interactions are negligible, the polarization is determined uniquely by the deformation. We also mention that $\boldsymbol{E}$ is not a freely varying parameter but is determined from Gauss's law; that is,

$$\mathrm{div}\boldsymbol{E} = \frac{1}{\epsilon_0}\,(\varrho_f - \mathrm{div}\boldsymbol{P}),$$

where ϵ_0 is the permittivity of free space, and ϱ_f is the density of free charges.

Before moving on, we pause to consider $\tilde{\boldsymbol{P}}$. It is certainly true for an isotropic distribution of chains, but—since polymer chains are essentially entropic springs with a minimum energy length of $r = 0$—even for a general stress-free distribution of chains, we expect that $\langle\tilde{\boldsymbol{r}}\rangle_{\tilde{\boldsymbol{r}}} = 0$. For any such reference distribution of chains, we find that, under the affine deformation assumption, the polarization vanishes for all $\boldsymbol{F}$. Indeed, since averaging is linear,

$$\tilde{\boldsymbol{P}} = N_0\left\langle\boldsymbol{M}\frac{\boldsymbol{F}\tilde{\boldsymbol{r}}}{b}\right\rangle_{\tilde{\boldsymbol{r}}} = \frac{N_0}{b}\boldsymbol{M}\boldsymbol{F}\,\langle\tilde{\boldsymbol{r}}\rangle_{\tilde{\boldsymbol{r}}} = \boldsymbol{0}.$$

It would seem then that our model, at least thus far, is not very interesting. More precisely, this model does not give rise to piezoelectricity. This is also reassuring in the sense that a conventional elastomer is indeed not piezoelectric; however, we will (in due course), aside from flexoelectricity, be able to comment on the precise conditions for the design of emergent piezoelectricity as well.

Flexoelectricity and the Elastomer Unit Cell

Moving forward, we will be interested in the polarization as a function of $\mathrm{Grad}\,\boldsymbol{F}$, where $\boldsymbol{F}$ is the deformation gradient; that is, we are interested in $\tilde{\boldsymbol{P}} = \tilde{\boldsymbol{P}}(\mathrm{Grad}\,\boldsymbol{F})$ and whether or not this relationship is as trivial as the polarization as a function of merely $\boldsymbol{F}$. The $\mathrm{Grad}\,\boldsymbol{F}$ term could, for instance, be the result of a bending deformation and, hence, result in flexoelectricity. To model the effects of $\mathrm{Grad}\,\boldsymbol{F}$ at a material point, we must now think beyond the probability distribution of $\tilde{\boldsymbol{r}}$ and consider also the geometry of the unit cell.

Prior work [mentioned in the previous section (74, 78, 87–89)] which developed and made use of a unit cell in the reference configuration in order to relate continuum-scale deformations to chain-scale deformations was focused primarily on the statistical distribution of chain end-to-end vectors and the choice of kinematic assumption. To the authors' knowledge, the geometry of the unit cell was not ever considered significant in and of itself (other than to ensure that $\tilde{r} = b\sqrt{n}$ for all $\tilde{\boldsymbol{r}}$). We are therefore in the position of being interested in defining a unit cell geometry but of being more or less without precedent. Therefore, as a first example, we will assign dimensions to the Arruda–Boyce eight-chain model (or rather, determine the dimensions and let them have physical significance) (see refs. 76 and 77, for example). The unit cell Fig. 2*A* consists of eight chains, each emanating from the center of the cell to one of the eight corners of the cube.

Each chain is assumed to satisfy $\tilde{r} = b\sqrt{n}$; thus, the length of an edge of the unit cell is $\ell := 2b\sqrt{n/3}$.[‖] The kinematic assumption that we now make—similar to the affine deformation assumption—will be that 1) the unit cell deforms under $\boldsymbol{F}$ (where $\boldsymbol{F}$ is allowed to vary throughout the cell) and 2) the beginning and end of the chain end-to-end vectors remain rigidly attached to their corresponding points in the unit cell. For the eight-chain model, this means that each of the end-to-end vectors, in the deformed configuration, still begins at the center of the cell and ends at its respective corner.

[¶] This follows, in part, because their nonlocal relationship at the chain scale simplifies to a local one (80).

[#] Historically, there has been some controversy related to this. The two most common kinematic assumptions are what we will refer to as the affine deformation assumption and the cooperative network assumption. In either case, the reference chains are arranged in a unit cell, and the cell is deformed in relation to the deformation gradient, $\boldsymbol{F}$. According to the affine deformation assumption, the chain end-to-end vectors in the reference configuration, $\tilde{\boldsymbol{r}}$, are mapped to the current configuration by $\boldsymbol{r} = \boldsymbol{F}\tilde{\boldsymbol{r}}$ (74), whereas, for the cooperative network assumption, the unit cell is first rotated such that its axes are aligned with the principal frame (76). Then the cell is deformed along each of its axes according to its respective principal stretch. In the context of both elasticity (74, 77) and electroelasticity (91, 92), there are important differences between the two assumptions, which can sometimes even lead to qualitatively different behaviors. In this work, we will focus on deformations which, in the frame of reference of interest, are such that $\boldsymbol{F}$ is diagonal. Thus, the two kinematic assumptions will be equivalent.

[‖] The length $b\sqrt{n}$ is motivated by random walk statistics. It is the most likely distance (from the starting point) for a random walk of n steps with step length b. Assuming all chains in the reference configuration have length $\tilde{r} = b\sqrt{n}$ is a standard assumption in the constitutive modeling of rubber (74, 76, 87–89).

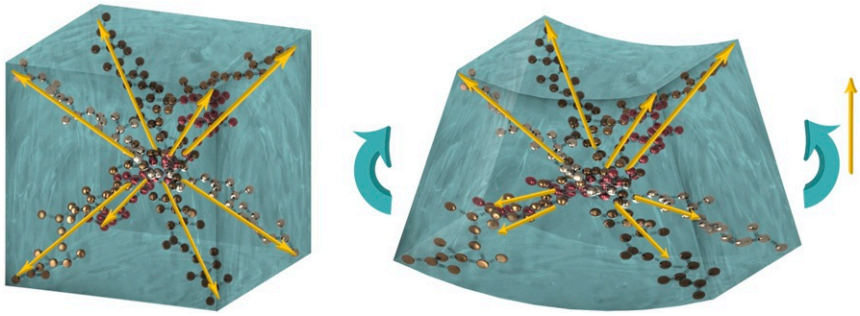

Fig. 2. Schematic of a unit cell of an eight-chain model in (*A*) reference and (*B*) deformed state upon bending. The yellow arrows indicate the chain polarization in both configurations. While the unit cell in the reference configuration is electrically neutral, the net polarization is upward in the deformed configuration under bending.

Having decided on an example unit cell, we next identify deformations of interest. As mentioned previously, we will limit our investigation, for the time being, to diagonal $\boldsymbol{F}$. In addition, since most elastomers are approximately incompressible, we will consider $\boldsymbol{F}$ such that $J=1$. Thus, let

$$\boldsymbol{F}(\boldsymbol{x})=\operatorname{diag}\left(\lambda_1(\boldsymbol{x}),\lambda_2(\boldsymbol{x}),\left(\lambda_1(\boldsymbol{x})\lambda_2(\boldsymbol{x})\right)^{-1}\right), \qquad [24]$$

where $\boldsymbol{x}$ is the position of a material point in the reference configuration. For ease of notation, let $\lambda_{i,j}:=\partial\lambda_i/\partial x_j$. Then, we assume $\boldsymbol{F}$ varies gradually enough relative to the size of a unit cell such that $\operatorname{Grad}\boldsymbol{F}$ is approximately constant. To be precise, we assume $\epsilon:=\max_{i,j}|\tilde{r}\lambda_{i,j}|\ll 1$. Next, let $\boldsymbol{y}$ denote a position within the eight-chain unit cell so that $y_i\in[x_i-\ell/2,x_i+\ell/2]$. Then, $\lambda_i(\boldsymbol{y})=\lambda_i(\boldsymbol{x})+\sum_{j=1}^{3}\lambda_{i,j}(\boldsymbol{x})y_j+\mathcal{O}(\epsilon^2)$. Neglecting $\mathcal{O}(\epsilon^2)$ terms, we have the result

$$\langle\boldsymbol{r}\rangle_{\boldsymbol{r}}=\frac{\tilde{r}}{3}\left(\tilde{r}\lambda_{1,1},\tilde{r}\lambda_{2,2},\alpha_3\right), \qquad [25]$$

where

$$\begin{aligned}\alpha_3=\frac{\sqrt{3}}{8}\sum_{i=1}^{2}\sum_{j=1}^{2}\sum_{k=1}^{2}\Bigg\{&(-1)^k\\&\times\left[\lambda_1+\frac{\tilde{r}}{\sqrt{3}}\left((-1)^i\lambda_{1,1}+(-1)^j\lambda_{1,2}+(-1)^k\lambda_{1,3}\right)\right]^{-1}\\&\times\left[\lambda_2+\frac{\tilde{r}}{\sqrt{3}}\left((-1)^i\lambda_{2,1}+(-1)^j\lambda_{2,2}+(-1)^k\lambda_{2,3}\right)\right]^{-1}\Bigg\}.\end{aligned}$$

The expression for α_3 is still complicated, however. To simplify further, and because we are ultimately interested in flexoelectricity, consider λ_1 and λ_2 of the form

$$\lambda_j=\overline{\lambda}_j+\lambda_{j,3}x_3, \qquad [26]$$

as this could correspond to a bending about some axis in the $\hat{\boldsymbol{e}}_1,\hat{\boldsymbol{e}}_2$ plane. In this case,

$$\langle\boldsymbol{r}\rangle_{\boldsymbol{r}}=\left(0,0,\frac{-3\tilde{r}^2\left(\overline{\lambda}_2\lambda_{1,3}+\overline{\lambda}_1\lambda_{2,3}\right)}{\left(3\overline{\lambda}_1{}^2-\tilde{r}^2\lambda_{1,3}^2\right)\left(3\overline{\lambda}_2{}^2-\tilde{r}^2\lambda_{2,3}^2\right)}\right), \qquad [27]$$

such that, in general, we have a nonzero polarization. Further, we can see from Eq. **22** that, if $\boldsymbol{M}=\mu\boldsymbol{I}$ (where $\boldsymbol{I}$ is the identity operator), then $\boldsymbol{P}$ is aligned (or antialigned) with $\operatorname{Grad}\lambda_1$ and $\operatorname{Grad}\lambda_2$ (i.e., the $\hat{\boldsymbol{e}}_3$ direction).

We can make the following observations regarding Eq. **27**.

1) It is interesting to see, in Eq. **27**, that $\langle\boldsymbol{r}\rangle_{\boldsymbol{r}}$ can diverge if $3\overline{\lambda}_1{}^2=\tilde{r}^2\lambda_{1,3}^2$ or $3\overline{\lambda}_2{}^2=\tilde{r}^2\lambda_{2,3}^2$. For this to occur, roughly speaking, the deformation gradient $\boldsymbol{F}$ must change appreciably relative to the size of the unit cell (more precisely, $\tilde{r}\lambda_{i,3}=\mathcal{O}(1)$). This violates a prior assumption, and so it should not be surprising that it leads to nonphysical results. If $\boldsymbol{F}$ changes appreciably relative to the size of the unit cell, then perhaps our unit cell is too large or we need to resort to a different modeling approach altogether.
2) It is also interesting that, if $\overline{\lambda}_2\lambda_{1,3}=-\overline{\lambda}_1\lambda_{2,3}$, then $\tilde{\boldsymbol{P}}$ vanishes. This is, in part, because of incompressibility. Indeed, let λ_3 denote the stretch in the $\hat{\boldsymbol{e}}_3$ direction. Then,

$$\lambda_3=\left(\overline{\lambda}_1\overline{\lambda}_2+\left(\overline{\lambda}_2\lambda_{1,3}+\overline{\lambda}_1\lambda_{2,3}\right)x_3+\lambda_{1,3}\lambda_{2,3}x_3^2\right)^{-1},$$

such that $\left(\overline{\lambda}_2\lambda_{1,3}+\overline{\lambda}_1\lambda_{2,3}\right)=0$ implies $\lambda_3(x_3)$ is an even function, and, therefore, all of the chains experience the same stretch in the $\hat{\boldsymbol{e}}_3$ direction.
3) To see how the flexoelectric effect scales with stretch, consider $\overline{\lambda}_3:=\left(\overline{\lambda}_1\overline{\lambda}_2\right)^{-1}$. Neglecting $\mathcal{O}(\epsilon^2)$ terms in the denominator of Eq. **27** results in $\tilde{P}_3\sim\mathcal{O}\left(\left(\overline{\lambda}_2\lambda_{1,3}+\overline{\lambda}_1\lambda_{2,3}\right)\overline{\lambda}_3^2\right)$. As a result, we see that our theory agrees with the surprising experimental result that prestretching the elastomer in the direction of $\operatorname{Grad}\boldsymbol{F}$ can lead to giant flexoelectricity (93). Note that, if $\overline{\lambda}_1=\overline{\lambda}_2=\overline{\lambda}_3^{-1/2}$, then this enhancement scales as $\overline{\lambda}_3^{3/2}$; however, if $1=\overline{\lambda}_1\gg\overline{\lambda}_2=\overline{\lambda}_3^{-1}$ (or vice versa), then the enhancement is quadratic in $\overline{\lambda}_3$.

Elastomer Design and the Conditions for the Piezoelectric Effect

Although not the primary focus of the current work, since piezoelectricity is arguably the most well-known and direct form of electromechanical coupling, it would be illuminating to understand the precise conditions under which an elastomer can be designed to exhibit such a property. We emphasize once again that, while flexoelectricity is universal, piezoelectricity is not, and we know of no piezoelectric elastomers.** To make progress on this, we assume that $\boldsymbol{M}$ differs from chain to chain. By doing so, from Eq. **22**, the polarization becomes

$$\tilde{\boldsymbol{P}}=J\boldsymbol{P}=JN\langle\boldsymbol{p}\rangle_{\boldsymbol{r}}=N_0\left\langle\boldsymbol{M}\frac{\boldsymbol{r}}{b}\right\rangle_{\boldsymbol{r}}. \qquad [28]$$

A special case can be constructed by considering a relation of $\boldsymbol{M}^{(2)}=-\boldsymbol{M}^{(1)}$ in which $\boldsymbol{M}^{(1)}$ ($\boldsymbol{M}^{(2)}$) belongs to the upper (lower) half of chains in the $\hat{\boldsymbol{e}}_3$ direction of the eight-chain model, as shown in Fig. 3.

**Certain polymers—but not elastomers—do exhibit piezoelectricity, such as PVDF (94) and polymer–ceramic composites (95).

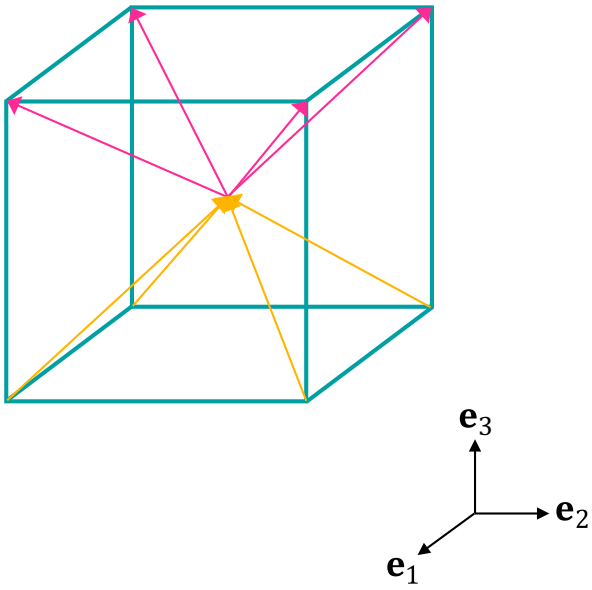

Fig. 3. Schematic of an eight-chain model exhibiting piezoelectric behavior. The arrows show the direction of the polarization of each chain.

Here, by considering the eight-chain model, we are assuming that the system is isotropic from a mechanical (elastic) perspective, while the linear transformation $\boldsymbol{M}$ is not unique in the entire cell and thus not isotropic from an electrostatic point of view. This assumption gives us a nonvanishing polarization, even in the reference configuration.

We consider a deformation which varies along the unit cell; that is, $\lambda_i(\boldsymbol{y}) = \lambda_i(\boldsymbol{x}) + \sum_{j=1}^{3} \lambda_{i,j}(\boldsymbol{x}) y_j + \mathcal{O}(\epsilon^2)$. Based on the model we introduced for flexoelectricity in previous section, we obtain

$$\begin{aligned}\langle \boldsymbol{M}\boldsymbol{r}\rangle_{\boldsymbol{r}} &= \frac{1}{2}\left[\left\langle \boldsymbol{M}^{(1)}\boldsymbol{r}\right\rangle_{\boldsymbol{r}} + \left\langle \boldsymbol{M}^{(2)}\boldsymbol{r}\right\rangle_{\boldsymbol{r}}\right] \\ &= \boldsymbol{M}^{(1)}\frac{\tilde{r}}{3}(0,0,\alpha_3),\end{aligned}$$

where

$$\begin{aligned}\alpha_3 = \frac{\sqrt{3}}{8}\sum_{i=1}^{2}\sum_{j=1}^{2}\sum_{k=1}^{2} \\ \left\{\left[\lambda_1 + \frac{\tilde{r}}{\sqrt{3}}\left((-1)^i\lambda_{1,1} + (-1)^j\lambda_{1,2} + (-1)^k\lambda_{1,3}\right)\right]^{-1}\right. \\ \left.\times\left[\lambda_2 + \frac{\tilde{r}}{\sqrt{3}}\left((-1)^i\lambda_{2,1} + (-1)^j\lambda_{2,2} + (-1)^k\lambda_{2,3}\right)\right]^{-1}\right\}.\end{aligned}$$

Again, our ultimate goal is to investigate flexoelectricity. Therefore, restricting our attention to the bending about some axis in the $\hat{\boldsymbol{e}}_1, \hat{\boldsymbol{e}}_2$ plane the same as Eq. **26**, we obtain the net polarization after the deformation of the unit cell as follows:

$$\begin{aligned}\tilde{\boldsymbol{P}} &= N_0\left\langle \boldsymbol{M}\frac{\boldsymbol{r}}{b}\right\rangle_{\boldsymbol{r}} \\ &= N_0\boldsymbol{M}^{(1)}\left(0,0,\frac{\sqrt{3}\tilde{r}\left(3\overline{\lambda}_1\overline{\lambda}_2 + \tilde{r}^2\lambda_{1,3}\lambda_{2,3}\right)}{\left(3\overline{\lambda}_1{}^2 - \tilde{r}^2\lambda_{1,3}^2\right)\left(3\overline{\lambda}_2{}^2 - \tilde{r}^2\lambda_{2,3}^2\right)}\right)^T.\end{aligned}$$

Here, there are few observations that can be made.

1) The net polarization after the deformation has contributions from two different types of deformations. The first term (in the numerator) is from the deformation gradient itself, which is an indication of the piezoelectric effect; meanwhile, the second term originates from the gradients of the deformation gradient, which is an indication of the flexoelectric behavior.
2) By assumption, $\max_j |\tilde{r}\lambda_{j,3}| = \mathcal{O}(\epsilon)$ is small. Thus, the second term, which is attributed to the flexoelectric effect, is much smaller than the flexoelectric response of the electrically isotropic case in the previous section (to be precise, it is $\mathcal{O}(\epsilon^2)$ compared to $\mathcal{O}(\epsilon)$). The conclusion is that, in this case, while we have increased the piezoelectric effect, it has been at the expense of flexoelectricity.
3) Similar to the previous setup of the unit cell, stretching the unit cell in the $\hat{\boldsymbol{e}}_3$ direction can enhance both piezoelectric and flexoelectric response in a linear and quadratic way, respectively.

The Design of Elastomers for Emergent Flexoelectricity

Clearly, we should maximize the spectral radius of $\boldsymbol{M}$ if we aim to maximize the flexoelectric effect. For the case of a fixed dipole rigidly attached to each monomer (i.e., $\boldsymbol{M} = \mu\boldsymbol{Q}$), this amounts to maximizing the magnitude of the dipoles, μ. We could potentially engage in such a design process (computationally) by using density functional theory (see ref. 96, for example). However, we also note that it is often trivial to increase the density of cross-links in an elastomer. In addition, we could theoretically influence the alignment of chains in the network by weakly cross-linking, applying an external electric field, and then cross-linking further. Therefore, it is also conceivable that the unit cell itself can be taken as a design variable (80). This may prove to be a fruitful endeavor, since, for elastomers that consist of the type of polymer chains considered herein, the geometry of the unit cell and the arrangement of chains within the unit cell influence the magnitude and direction of the flexoelectric effect.

The main goal that we now focus on is to design an elastomer unit cell to tune the flexoelectric response. In particular, we propose (in analogy with the dominant role a dipole moment plays in the phenomenon of piezoelectricity) that flexoelectricity is primarily dictated by the next-order multipole expansion term—the quadrupolar moment. In particular, we anticipate unit cells with large variations to have a stronger flexoelectric

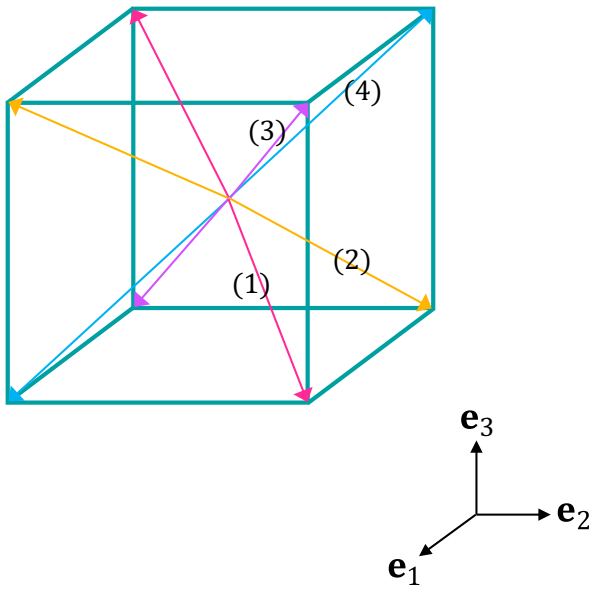

Fig. 4. Design of an eight-chain unit cell to tune the flexoelectric response. Polymers are paired together through an inversion symmetry as shown by numbers, and, when the electrical properties of the four pairs are tuned to maximize the gradient of the quadruple moment of the unit cell, the flexoelectric response is stretch invariant.

response. The quadrupole moment can be constructed from two dipole moments in opposite directions. The quadrupole moment ($\mathcal{Q}$) is a second-order moment of charges and can be formulated as (97)

$$\mathcal{Q} = \sum_{i=1}^{n} \left[3\mathbf{x}_i \otimes \mathbf{x}_i - |\mathbf{x}_i|^2 \mathbb{I}\right] q_i, \qquad [29]$$

where the sum is over all discrete charges (q_i), $\mathbf{x}_i$ is the position vector of the charge q_i, and $\mathbb{I}$ is the identity matrix. Analogous to the fact that dipole distribution can be architected to design materials with high piezoelectricity, quadrupole moment and its gradient can play the same role in designing giant flexoelectric materials.

Here we aim to establish a reference unit cell with vanishing net polarization but finite quadrupole moment and its gradient. We claim that the higher gradient in quadrupole moment will result in higher flexoelectric effect. The simplest example can be achieved by enforcing an inversion symmetry about the center of the eight-chain unit cell (as shown in Fig. 4), which leaves four pairs of chains, each with a different $\boldsymbol{M}$ and each acting as a quadrupole moment.

We make the choice

$$\boldsymbol{M} = \frac{1}{K_1}\boldsymbol{M}^{(1)} = \frac{1}{K_2}\boldsymbol{M}^{(2)} = \frac{1}{K_3}\boldsymbol{M}^{(3)} = \frac{1}{K_4}\boldsymbol{M}^{(4)},$$

where K_i ($i = 1:4$) are some arbitrary real numbers. Again, consider a deformation gradient of the form Eq. **24** and its associated assumptions. By restricting the deformation to the bending of the unit cell similar to Eq. **26**, the polarization after the deformation is obtained as

$$\tilde{\boldsymbol{P}} = \sum_i \frac{N_0^{(i)}}{b} \left\langle \boldsymbol{M}^{(i)} \boldsymbol{r}^{(i)} \right\rangle_{\boldsymbol{r}} = \frac{N_0}{b} \boldsymbol{M}^{(1)} \tilde{r}^2 \, (\alpha_1, \alpha_2, \alpha_3),$$

where α_i are defined as

$$\alpha_1 = \frac{1}{12}(K_2 + K_3 - K_1 - K_4)\lambda_{1,3},$$
$$\alpha_2 = \frac{1}{12}(K_3 + K_4 - K_1 - K_2)\lambda_{2,3},$$
$$\alpha_3 = \frac{-3(K_1 + K_2 + K_3 + K_4)\left(\overline{\lambda}_2 \lambda_{1,3} + \overline{\lambda}_1 \lambda_{2,3}\right)}{4\left(3\overline{\lambda}_1{}^2 - \tilde{r}^2\lambda_{1,3}^2\right)\left(3\overline{\lambda}_2{}^2 - \tilde{r}^2\lambda_{2,3}^2\right)}.$$

Upon a closer examination, we notice that the third term is exactly the flexoelectricity constant we obtained in Eq. **27** for the case $K_1 = K_2 = K_3 = K_4 = 1$, which is equivalent to the electrically isotropic case.

However, if we allow the K_i to vary, we see that we can obtain flexoelectricity in the plane orthogonal to $\hat{\boldsymbol{e}}_3$. Indeed, if we make the choice $K_1 = K_4 = -K_2 = -K_3$, this results in enhancing the α_1 while eliminating α_3. Interestingly, we see that, in this case, the flexoelectric effect is invariant with respect to $\overline{\lambda}_1$ and $\overline{\lambda}_2$. This property may be particularly useful for applications in soft sensors and robotics where we may expect finite stretches to occur but would prefer the flexoelectric response to remain constant, or, at the very least, not diminish.

Concluding Remarks

In this work, we have established the mechanisms (and the underlying theory) underpinning flexoelectricity in elastomers. Surprisingly, our theory shows that giant flexoelectricity can be attained in incompressible elastomers by prestretching the material in the strain gradient direction. In particular, the scaling of the flexoelectric effect with respect to prestretch is at least superlinear (with exponent $3/2$) and, for certain loading conditions, can scale quadratically with prestretch. This suggests a facile route to achieve high-output energy harvesting and high-fidelity soft sensors.

We also considered the design of the polymer network architecture. By poling the chains (e.g., using an applied electric field), we can develop a piezoelectric elastomer. This piezoelectricity is at expense of the flexoelectric effect which diminishes in the poled architecture. The emergent flexoelectric effect can also be 1) made stretch invariant, and 2) tuned in different directions relative to the direction of the strain gradient by adjusting the quadrupolar moment of the material unit cell. Stretch invariance may prove useful for soft sensors, and the tunable nature of the flexoelectric direction may be useful for producing soft robots with larger degree-of-freedom actuators.

Data Availability. All study data are included in the article and *SI Appendix*.

ACKNOWLEDGMENTS. K.M. and P.S. were supported by the University of Houston and the M.D. Anderson Professorship. P.S. and M.G. gratefully acknowledge encouragement by and discussions with Professor Kaushik Dayal. M.G. thanks Professors Prashant Purohit and Gal de Botton for insightful discussions.

1. C. Keplinger, T. Li, R. Baumgartner, Z. Suo, S. Bauer, Harnessing snap-through instability in soft dielectrics to achieve giant voltage-triggered deformation. *Soft Matter* **8**, 285–288 (2012).
2. J.-Y. Sun *et al.*, Highly stretchable and tough hydrogels. *Nature* **489**, 133–136 (2012).
3. J. W. Kwak *et al.*, Wireless sensors for continuous, multimodal measurements at the skin interface with lower limb prostheses. *Sci. Transl. Med.* **12**, eabc4327 (2020).
4. J. A. Rogers, T. Someya, Y. Huang, Materials and mechanics for stretchable electronics. *Science* **327**, 1603–1607 (2010).
5. Q. Zhang, Q. Liang, J. A. Rogers, Water-soluble energy harvester as a promising power solution for temporary electronic implants. *APL Mater.* **8**, 120701 (2020).
6. R. Zhao, Y. Kim, S. A. Chester, P. Sharma, X. Zhao, Mechanics of hard-magnetic soft materials. *J. Mech. Phys. Solid.* **124**, 244–263 (2019).
7. Q. Ze *et al.*, Magnetic shape memory polymers with integrated multifunctional shape manipulation. *Adv. Mater.* **32**, 1906657 (2020).
8. S. Xu *et al.*, Soft microfluidic assemblies of sensors, circuits, and radios for the skin. *Science* **344**, 70–74 (2014).
9. S.-K. Kang *et al.*, Bioresorbable silicon electronic sensors for the brain. *Nature* **530**, 71–76, 2016.
10. D.-H. Kim *et al.*, Thin, flexible sensors and actuators as 'instrumented' surgical sutures for targeted wound monitoring and therapy. *Small* **8**, 3263–3268 (2012).
11. D.-H. Kim *et al.*, Epidermal electronics. *Science* **333**, 838–843 (2011).
12. M. Han *et al.*, Three-dimensional piezoelectric polymer microsystems for vibrational energy harvesting, robotic interfaces and biomedical implants. *Nat. Electron.* **2**, 26–35 (2019).
13. A. Erturk, D. J. Inman, *Piezoelectric Energy Harvesting* (John Wiley, 2011).
14. K. Nan *et al.*, Compliant and stretchable thermoelectric coils for energy harvesting in miniature flexible devices. *Sci. Adv.* **4**, eaau5849 (2018).
15. K. S. Kim *et al.*, Large-scale pattern growth of graphene films for stretchable transparent electrodes. *Nature* **457**, 706–710 (2009).
16. D.-Y. Khang, H. Jiang, Y. Huang, J. A. Rogers, A stretchable form of single-crystal silicon for high-performance electronics on rubber substrates. *Science* **311**, 208–212 (2006).
17. S. Xu *et al.*, Stretchable batteries with self-similar serpentine interconnects and integrated wireless recharging systems. *Nat. Commun.* **4**, 1543 (2013).
18. Y. Kim, H. Yuk, R. Zhao, S. A. Chester, X. Zhao, Printing ferromagnetic domains for untethered fast-transforming soft materials. *Nature* **558**, 274–279 (2018).
19. K. J. Kim, S. Tadokoro, *Electroactive Polymers for Robotic Applications (Artificial Muscles and Sensors,* Springer, 2007), vol. 23.
20. Y. Kim, G. A. Parada, S. Liu, X. Zhao, Ferromagnetic soft continuum robots. *Sci. Robot.* **4**, eaax7329 (2019).
21. G. M. Sessler, J. Hillenbrand, "Electromechanical response of cellular electret films" in *10th International Symposium on Electrets (ISE 10)*. Proceedings, A. A. Konsta, A. Vasilikou-Dova, K. Vartzeli-Nikaki, Eds. (Institute of Electrical and Electronics Engineers, 1999), pp. 261–264.
22. G. M. Sessler, "Physical principles of electrets" in *Electrets*, G. M. Sessler, Ed. (Springer, 1980), pp. 13–80.
23. M. Wegener, S. Bauer, Microstorms in cellular polymers: A route to soft piezoelectric transducer materials with engineered macroscopic dipoles. *ChemPhysChem* **6**, 1014–1025 (2005).
24. G. Buchberger, R. Schwödiauer, S. Bauer, Flexible large area ferroelectret sensors for location sensitive touchpads. *Appl. Phys. Lett.* **92**, 123511 (2008).
25. Q. Deng, L. Liu, P. Sharma, Electrets in soft materials: Nonlinearity, size effects, and giant electromechanical coupling. *Phys. Rev.* **90**, 012603 (2014).

26. L. Liu, P. Sharma, Emergent electromechanical coupling of electrets and some exact relations—The effective properties of soft materials with embedded external charges and dipoles. *J. Mech. Phys. Solid.* **112**, 1–24 (2018).
27. F. Darbaniyan, K. Dayal, L. Liu, P. Sharma, Designing soft pyroelectric and electrocaloric materials using electrets. *Soft Matter* **15**, 262–277 (2019).
28. F. Darbaniyan, K. Mozaffari, L. Liu, P. Sharma, Soft matter mechanics and the mechanisms underpinning the infrared vision of snakes. *Matter* **4**, 241–252 (2021).
29. A. Apte *et al.*, 2D electrets of ultrathin moO_2 with apparent piezoelectricity. *Adv. Mater.* **32**, 2000006 (2020).
30. A. Mellinger, M. Wegener, W. Wirges, R. Reddy. Mallepally, R. Gerhard-Multhaupt, Thermal and temporal stability of ferroelectret films made from cellular polypropylene/air composites. *Ferroelectrics* **331**, 189–199 (2006).
31. S. Krichen, P. Sharma, Flexoelectricity: A perspective on an unusual electromechanical coupling. *J. Appl. Mech.* **83**, 030801 (2016).
32. Q. Deng, L. Liu, P. Sharma, "A continuum theory of flexoelectricity" in *Flexoelectricity in Solids: From Theory to Applications*, P. V. Yudin, A. Tagantsev, Eds. (World Scientific, 2017), pp. 111–167.
33. T. D. Nguyen, S. Mao, Y.-W. Yeh, P. K. Purohit, M. C. McAlpine, Nanoscale flexoelectricity. *Adv. Mater.* **25**, 946–974 (2013).
34. N. D. Sharma, C. M. Landis, P. Sharma, Piezoelectric thin-film superlattices without using piezoelectric materials. *J. Appl. Phys.* **108**, 024304 (2010).
35. J. Fousek, L. E. Cross, D. B. Litvin, Possible piezoelectric composites based on the flexoelectric effect. *Mater. Lett.* **39**, 287–291 (1999).
36. B. Chu, W. Zhu, N. Li, L. E. Cross, Flexure mode flexoelectric piezoelectric composites. *J. Appl. Phys.* **106**, 104109 (2009).
37. B. Wang, S. Yang, P. Sharma, Flexoelectricity as a universal mechanism for energy harvesting from crumpling of thin sheets. *Phys. Rev. B* **100**, 035438 (2019).
38. Q. Deng, M. Kammoun, A. Erturk, P. Sharma, Nanoscale flexoelectric energy harvesting. *Int. J. Solid Struct.* **51**, 3218–3225 (2014).
39. X. Jiang, W. Huang, S. Zhang, Flexoelectric nano-generator: Materials, structures and devices. *Nano Energy* **2**, 1079–1092 (2013).
40. M. S. Majdoub, P. Sharma, T. Çağin, Dramatic enhancement in energy harvesting for a narrow range of dimensions in piezoelectric nanostructures. *Phys. Rev. B* **78**, 121407 (2008). Erratum in: *Phys. Rev. B* **79**, 159901 (2009).
41. A. H. Rahmati, S. Bauer, P. Sharma, Nonlinear bending deformation of soft electrets and prospects for engineering flexoelectricity and transverse (d_{31}) piezoelectricity. *Soft Matter* **15**, 127–148 (2019).
42. S.-B. Choi, G.-W. Kim, Measurement of flexoelectric response in polyvinylidene fluoride films for piezoelectric vibration energy harvesters. *J. Phys. Appl. Phys.* **50**, 075502 (2017).
43. U. K. Bhaskar *et al.*, Flexoelectric MEMS: Towards an electromechanical strain diode. *Nanoscale* **8**, 1293–1298 (2016).
44. U. K. Bhaskar *et al.*, A flexoelectric microelectromechanical system on silicon. *Nat. Nanotechnol.* **11**, 263–266 (2016).
45. Z. Wang *et al.*, Giant flexoelectric polarization in a micromachined ferroelectric diaphragm. *Adv. Funct. Mater.* **23**, 124–132 (2013).
46. A. Abdollahi, I. Arias, Constructive and destructive interplay between piezoelectricity and flexoelectricity in flexural sensors and actuators. *J. Appl. Mech.* **82**, 121003 (2015).
47. Q. Deng, F. Ahmadpoor, W. E Brownell, P. Sharma, The collusion of flexoelectricity and Hopf bifurcation in the hearing mechanism. *J. Mech. Phys. Solid.* **130**, 245–261 (2019).
48. W. E. Brownell, A. A. Spector, R. M. Raphael, A. S. Popel, Micro-and nanomechanics of the cochlear outer hair cell. *Annu. Rev. Biomed. Eng.* **3**, 169–194 (2001).
49. K. D. Breneman, W. E. Brownell, R. D. Rabbitt, Hair cell bundles: Flexoelectric motors of the inner ear. *PloS One* **4**, e5201 (2009).
50. Q. Deng, L. Liu, P. Sharma, Flexoelectricity in soft materials and biological membranes. *J. Mech. Phys. Solid.* **62**, 209–227 (2014).
51. X. Wen, D. Li, K. Tan, Q. Deng, S. Shen, Flexoelectret: An electret with a tunable flexoelectriclike response. *Phys. Rev. Lett.* **122**, 148001 (2019).
52. R. Maranganti, N. D. Sharma, P. Sharma, Electromechanical coupling in nonpiezoelectric materials due to nanoscale nonlocal size effects: Green's function solutions and embedded inclusions. *Phys. Rev. B* **74**, 014110 (2006).
53. D. Codony, P. Gupta, O. Marco, I. Arias, Modeling flexoelectricity in soft dielectrics at finite deformation. *J. Mech. Phys. Solid.* **146**, 104182 (2021).
54. A. Abdollahi, C. Peco, D. Millan, M. Arroyo, I. Arias, Computational evaluation of the flexoelectric effect in dielectric solids. *J. Appl. Phys.* **116**, 093502 (2014).
55. J. Yvonnet, L. P. Liu, A numerical framework for modeling flexoelectricity and maxwell stress in soft dielectrics at finite strains. *Comput. Methods Appl. Mech. Eng.* **313**, 450–482 (2017).
56. T. Q. Thai, X. Zhuang, H. S. Park, T. Rabczuk, A staggered explicit-implicit isogeometric formulation for large deformation flexoelectricity. *Eng. Anal. Bound. Elem.* **122**, 1–12 (2021).
57. A. K. Tagantsev, Piezoelectricity and flexoelectricity in crystalline dielectrics. *Phys. Rev. B* **34**, 5883 (1986).
58. R. Maranganti, P. Sharma, Atomistic determination of flexoelectric properties of crystalline dielectrics. *Phys. Rev. B* **80**, 054109 (2009).
59. M. Stengel, Flexoelectricity from density-functional perturbation theory. *Phys. Rev. B* **88**, 174106 (2013).
60. M. Stengel, Surface control of flexoelectricity. *Phys. Rev. B* **90**, 201112 (2014).
61. C. E. Dreyer, M. Stengel, D. Vanderbilt, Current-density implementation for calculating flexoelectric coefficients. *Phys. Rev. B* **98**, 075153 (2018).
62. P.-G. DeGennes, J. Prost, *The Physics of Liquid Crystals* (International Series of Monographs on Physics, Oxford University Press, 1993), vol. 83.
63. R. B. Meyer, Piezoelectric effects in liquid crystals. *Phys. Rev. Lett.* **22**, 918 (1969).
64. M. Kothari, M.-H. Cha, K.-S. Kim, Critical curvature localization in graphene. I. Quantum-flexoelectricity effect. *Proc. Math. Phys. Eng. Sci.* **474**, 20180054 (2018).
65. M. Kothari, M.-H. Cha, V. Lefevre, K.-S. Kim, Critical curvature localization in graphene. II. Non-local flexoelectricity–dielectricity coupling. *Proc. R. Soc. A* **475**, 20180671 (2019).
66. A. G. Kvashnin, P. B. Sorokin, B. I. Yakobson, Flexoelectricity in carbon nanostructures: Nanotubes, fullerenes, and nanocones. *J. Phys. Chem. Lett.* **6**, 2740–2744 (2015).
67. F. Ahmadpoor, P. Sharma, Flexoelectricity in two-dimensional crystalline and biological membranes. *Nanoscale* **7**, 16555–16570 (2015).
68. S. Kumar, D. Codony, I. Arias, P. Suryanarayana, Flexoelectricity in atomic monolayers from first principles. *Nanoscale* **13**, 1600–1607 (2021).
69. A. S. Banerjee, P. Suryanarayana, Cyclic density functional theory: A route to the first principles simulation of bending in nanostructures. *J. Mech. Phys. Solid.* **96**, 605–631 (2016).
70. M. Marvan, A. Havránek, Static volume flexoelectric effect in a model of linear chains. *Solid State Commun.* **101**, 493–496 (1997).
71. M. Marvan, A. Havránek, "Flexoelectric effect in elastomers" in *Relationships of Polymeric Structure and Properties*, I.Chudáček, Ed. (Springer, 1998), pp. 33–36.
72. S. Baskaran, X. He, Y. Wang, J. Y. Fu, Strain gradient induced electric polarization in α-phase polyvinylidene fluoride films under bending conditions. *J. Appl. Phys.* **111**, 014109 (2012).
73. B. Chu, D. R. Salem, Flexoelectricity in several thermoplastic and thermosetting polymers. *Appl. Phys. Lett.* **101**, 103905 (2012).
74. L. R. G. Treloar, *The Physics of Rubber Elasticity* (Oxford University Press, 1975).
75. P. J. Flory, Network structure and the elastic properties of vulcanized rubber. *Chem. Rev.* **35**, 51–75 (1944).
76. E. M. Arruda, M. C. Boyce, A three-dimensional constitutive model for the large stretch behavior of rubber elastic materials. *J. Mech. Phys. Solid.* **41**, 389–412 (1993).
77. M. C. Boyce, E. M. Arruda, Constitutive models of rubber elasticity: A review. *Rubber Chem. Technol.* **73**, 504–523 (2000).
78. N. Cohen, G. DeBotton, Electromechanical interplay in deformable dielectric elastomer networks. *Phys. Rev. Lett.* **116**, 208303 (2016).
79. M. Itskov, V. N. Khiêm, S. Waluyo, Electroelasticity of dielectric elastomers based on molecular chain statistics.*Math. Mech. Solid.* **24**, 862–873 (2018).
80. M. Grasinger, K. Dayal, Architected elastomer networks for optimal electromechanical response. *J. Mech. Phys. Solid.* **146**, 104171 (2020).
81. M. Grasinger, K. Dayal, Statistical mechanical analysis of the electromechanical coupling in an electrically-responsive polymer chain. *Soft Matter* **16**, 6265–6284 (2020).
82. W. Kuhn, F. Grün, Beziehungen zwischen elastischen konstanten und dehnungsdoppelbrechung hochelastischer stoffe. *Kolloid Z.* **101**, 248–271 (1942).
83. M. J. Lighthill, *An Introduction to Fourier Analysis and Generalised Functions* (Cambridge University Press, 1958).
84. G. Fredrickson *et al.*, *The Equilibrium Theory of Inhomogeneous Polymers* (International Series of Monographs on Physics, Oxford University Press on Demand, 2006), vol. 134.
85. D. R. Lide, *CRC Handbook of Chemistry and Physics* (CRC, ed. 85, 2004).
86. E. B. Tadmor, R. E. Miller, *Modeling Materials: Continuum, Atomistic and Multiscale Techniques* (Cambridge University Press, 2011).
87. H. M. James, E. Guth, Theory of the elastic properties of rubber. *J. Chem. Phys.* **11**, 455–481 (1943).
88. P. J. Flory, J. Rehner, Statistical mechanics of cross-linked polymer networks. II. *J. Chem. Phys.* **11**, 521–526 (1943).
89. P. D. Wu, E. Van Der Giessen, On improved network models for rubber elasticity and their applications to orientation hardening in glassy polymers. *J. Mech. Phys. Solid.* **41**, 427–456 (1993).
90. N. Cohen, K. Dayal, G. DeBotton, Electroelasticity of polymer networks. *J. Mech. Phys. Solid.* **92**, 105–126 (2016).
91. M. Grasinger, "Multiscale modeling and theoretical design of dielectric elastomers," PhD thesis, Carnegie Mellon University, Pittsburgh, PA (2019).
92. M. Grasinger, C. Majidi, K. Dayal, Nonlinear statistical mechanics drives intrinsic electrostriction and volumetric torque in polymer networks. *Phys. Rev. E* **103**, 042504 (2021).
93. S. Baskaran, X. He, Q. Chen, J. Y. Fu, Experimental studies on the direct flexoelectric effect in α-phase polyvinylidene fluoride films. *Appl. Phys. Lett.* **98**, 242901 (2011).
94. E. Fukada, S. Takashita, Piezoelectric effect in polarized poly (vinylidene fluoride). *Jpn. J. Appl. Phys.* **8**, 960 (1969).
95. K. K. Sappati, S. Bhadra, Piezoelectric polymer and paper substrates: A review. *Sensors* **18**, 3605 (2018).
96. M. K. Ashraf *et al.*, Theoretical design of bioinspired macromolecular electrets based on anthranilamide derivatives. *Biotechnol. Prog.* **25**, 915–922 (2009).
97. D. J. Griffiths, *Introduction to Electrodynamics* (Cambridge University Press, 2017).